Review article

Lu Sun, Yong Zhang, Yu He, Hongwei Wang and Yikai Su*

Subwavelength structured silicon waveguides and photonic devices

https://doi.org/10.1515/nanoph-2020-0070
Received January 30, 2020; revised March 27, 2020; accepted March 28, 2020

Abstract: Subwavelength structures such as subwavelength gratings (SWGs) and subwavelength metamaterials are capable of tailoring the optical properties of materials and controlling the flow of light at the nanoscale. The effective indices of the subwavelength structured strip and slab waveguides can be changed in a wide range by choosing an appropriate duty cycle or a filling factor of silicon, which provides an effective method to manipulate the optical field and achieve effective index matching for functional devices. Recent advances in nanofabrication techniques have made it possible to implement subwavelength structures in silicon strip and slab waveguides. Here we review various approaches used to design subwavelength structures and achieve exotic optical responses and discuss how these structures can be used to realize high-performance silicon photonic devices. Both one-dimensional SWG devices and two-dimensional subwavelength metamaterial devices are covered in this review, including subwavelength structure–based polarization handling devices, mode manipulation devices, and building blocks for integrated optical interconnects. Perspectives on subwavelength structured silicon photonic devices are also discussed.

Keywords: subwavelength structure; silicon photonics; metamaterial; polarization handling; mode multiplexing; optical interconnect.

***Corresponding author: Yikai Su,** State Key Lab of Advanced Optical Communication Systems and Networks, Department of Electronic Engineering, Shanghai Jiao Tong University, Shanghai 200240, China, e-mail: yikaisu@sjtu.edu.cn. https://orcid.org/0000-0002-1526-8187
Lu Sun, Yong Zhang, Yu He and Hongwei Wang: State Key Lab of Advanced Optical Communication Systems and Networks, Department of Electronic Engineering, Shanghai Jiao Tong University, Shanghai 200240, China

1 Introduction

Optical waveguides are fundamental elements in integrated optics. Essentially, all integrated devices are built on waveguides. To some extent, the properties of optical waveguides determine the performances of passive and active components, such as footprint, loss, crosstalk (CT), integration density, and so on. Structural design and refractive index engineering are important for the realization of novel and high-performance devices.

Silicon photonics has recently witnessed significant growth in academic research and industrial applications, mainly due to its compatibility with the complementary metal oxide semiconductor (CMOS) fabrication process. The high refractive index of silicon (~3.45) enables a high contrast relative to the surrounding cladding of a silicon waveguide and thus high confinement of the optical field. These properties are desirable for achieving densely integrated photonic circuits. A number of well-known silicon waveguides based on different structures have been demonstrated, including strip waveguide [1], slab waveguide [2], slot waveguide [3], and photonic crystal waveguide [4]. However, unlike other III–V materials whose refractive indices can be flexibly varied by using different constituent proportions, the refractive index of silicon is usually fixed, thus limiting the design freedom. Modal effective index matching and engineering are often needed in many devices, for example, couplers, polarization handling devices, and mode multiplexers. Therefore, it is highly desirable to find a methodology to change the effective refractive indices of silicon waveguides over a wide range through proper structural designs.

Subwavelength engineering is an effective way to vary the refractive index of a waveguide. It was first proposed to realize light coupling and mode conversion in one-dimensional (1D) subwavelength grating (SWG) waveguides [5]. In general, "subwavelength" refers to a structural period with which the Bragg reflection and diffraction effects are suppressed in the structure. By changing the period and duty cycle of an SWG, the effective index, dispersion, and optical field confinement

can be flexibly adjusted over a wide range. The SWG waveguide therefore exhibits exotic optical properties that cannot be realized with conventional waveguides. However, the fabrication of such waveguides should be considered carefully as the resolution and fabrication errors may greatly affect the device performance. In the telecom band centered at 1550 nm, the period of an SWG waveguide is typically around 300 nm, requiring a fine resolution of better than 90 nm if the duty cycle is set to 30%. In terms of fabrication, 193-nm deep ultraviolet (DUV) lithography has been widely used to define patterns on silicon-on-insulator (SOI) wafers [6, 7]. The lithographic resolution of 193-nm DUV light is typically 130 nm, which is smaller than the feature sizes of some subwavelength structures. Therefore, it can be used to fabricate some subwavelength structured devices. Thanks to the mass production capability of 193-nm DUV lithography, the average cost of a single device can be lowered with large quantity. However, for subwavelength structured silicon devices with smaller feature sizes, higher-resolution lithographic techniques are required, such as electron beam lithography (EBL) [8]. State-of-the-art EBL has enabled ~7-nm resolution in photoresist, and after dry etching, the minimum feature size of a device can reach ~40 nm. It usually results in more time and higher cost to define patterns using EBL, so EBL is mainly used for forward-looking research in laboratories. The development of fabrication technologies facilitates the research of SWG devices. A number of good review articles on SWG structures have appeared [9–11], providing comprehensive information from the principles to the applications.

Powered by advanced fabrication capabilities, recent years have seen a boom in subwavelength research not only in 1D SWG devices but also extending to two-dimensional (2D) index control in waveguides. This provides more freedom in optical field manipulation in the space domain, enabling new functional devices (e.g. mode converters) or improving the performances of integrated devices. In this article, we attempt to provide a general review of subwavelength structured waveguides and devices, covering the operation principle and the latest developments in device research. Section 2 introduces the optical properties of subwavelength structured waveguides. Section 3 reviews subwavelength structured polarization handling devices. Section 4 summarizes recent developments in mode converters and multiplexers. Section 5 discusses some building blocks for on-chip optical interconnects. Finally, section 6 concludes this review.

2 Optical properties of subwavelength structured waveguides

Subwavelength structured waveguides are waveguides that are segmented at a scale substantially smaller than the wavelength of the light propagating in the material. Here we discuss the behavior of the structure with the following two cases:

(a) For light propagating crosswise through a subwavelength structured waveguide as indicated by the blue arrows in Figure 1A, the angle θ_i of the diffraction order i is given by $n_d \sin\theta_i = i\lambda/\Lambda$, where n_d is the refractive index of the cladding or the substrate, λ is the wavelength of light in vacuum, and Λ is the period. If $\lambda/\Lambda > n_d$ and therefore $|\sin\theta_{\pm 1}| > 1$, the diffraction effects are suppressed for all the diffraction orders $|i| \geq 1$ [14].

(b) For light propagating lengthwise through a subwavelength structured waveguide as indicated by the green arrows in Figure 1A, the diffraction effects for all the diffraction orders including the Bragg reflection are suppressed if the period is smaller than the guided half-wavelength, that is, $\Lambda < \lambda/2n_{\text{eff}}$, where n_{eff} is the effective index of the Bloch–Floquet mode in the waveguide [10].

Therefore, in the subwavelength regime where the pitch is short enough, light propagates through subwavelength structured waveguides without radiation and Bragg reflection losses despite multiple discontinuities along the propagation direction. The subwavelength segments behave like an equivalent waveguide made of an artificial material, which can be fully described by the effective medium theory (EMT) [15, 16]. In this review, we focus on subwavelength structured waveguides built on the SOI platform, including segmented strip and slab waveguides. In strip-like waveguides, the subwavelength structures are arrayed along the propagation direction of light, acting as 1D strip waveguides with equivalent material refractive indices. In slab-like waveguides, the subwavelength structures are arranged along both directions of the plane, and the light propagates in all of the in-plane directions as in an equivalent slab waveguide. The optical properties of the two types of subwavelength structured waveguides are analyzed and discussed in the following.

To start with the simplest subwavelength structured waveguides, we consider an SWG that has subwavelength periodicity along a certain direction. It can comprise

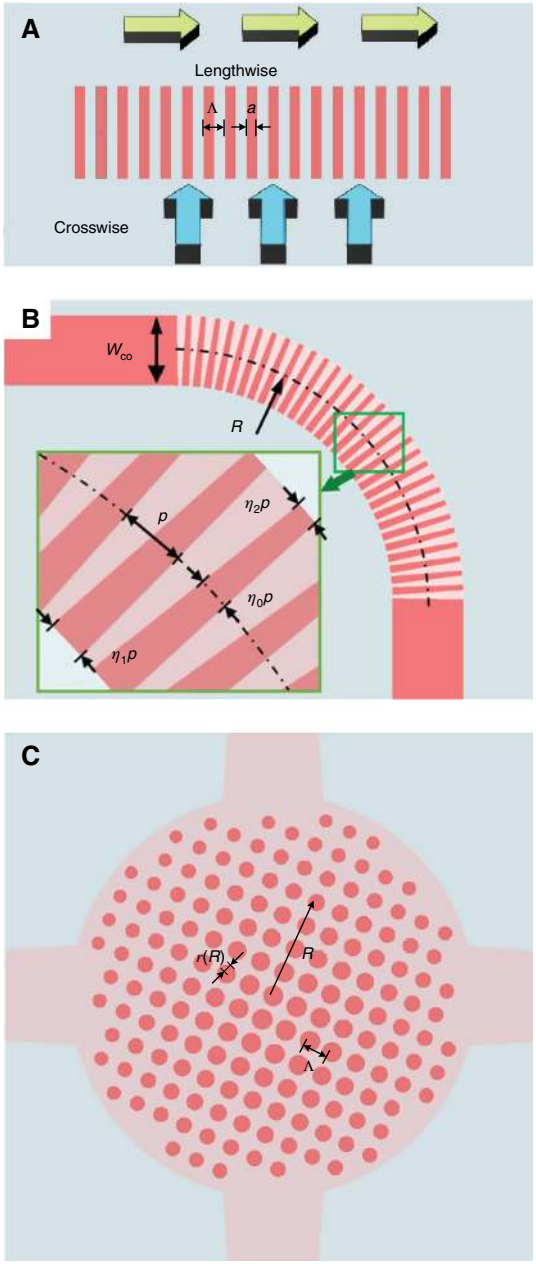

Figure 1: Schematic diagrams of various subwavelength structured strip and slab waveguides.
(A) SWG waveguide, (B) 90° waveguide bend, and (C) multimode crossing based on the subwavelength metamaterial. The red, pink, and gray colors represent silicon, partially etched silicon, and silica, respectively. B is reprinted from Wu et al. [12]. Copyright © 2019 by John Wiley and Sons. The structure in C was reported in Xu and Shi [13].

alternating strips of silicon and cladding material on the SOI platform (Figure 1A). A rigorous description of the periodic structure requires the Bloch–Floquet modal analysis for which a number of numerical solvers have been developed, including MIT Photonic Bands, Rsoft BandSolve, Lumerical FDTD Solution, and Photon Design CrystalWave [17–19]. However, many geometrical parameters of the subwavelength structures need to be optimized to achieve the desirable device performance, which is very time-consuming when using numerical solvers. To speed up the optimization process, people first use the EMT to simplify the physical model and obtain an estimation of the interval where the optimal parameters may be located. In this way, the parameter space is narrowed, and then one can search for the optimal parameters with numerical solvers. So the EMT is of central importance in designing subwavelength structured devices. For periodic pitches in the deep subwavelength regime ($\Lambda \ll \lambda$), the structure can be treated as a homogeneous waveguide made of an equivalent birefringent material, which was first studied by Rytov [20] in the 1950s. According to the EMT, the refractive indices of the equivalent material for polarizations parallel and perpendicular to the interfaces between the alternating layers can be approximated by the Rytov's formulas [20]:

$$\begin{aligned} n_{\parallel}^2 &= f n_{\mathrm{Si}}^2 + (1-f) n_{\mathrm{clad}}^2, \\ \frac{1}{n_{\perp}^2} &= f \frac{1}{n_{\mathrm{Si}}^2} + (1-f) \frac{1}{n_{\mathrm{clad}}^2}, \end{aligned} \tag{1}$$

where $f = a/\Lambda$ is the duty cycle of the grating structure, and n_{Si}, n_{clad} are the refractive indices of silicon and the cladding material, respectively. The results obtained from the equations agree well with those derived from the Bloch–Floquet modal analysis. The geometry of the SWG provides precise control over the effective index and therefore modal confinement, dispersion, and birefringence, which will be discussed in detail later. The EMT is also applicable to other subwavelength structured waveguides such as the 90° waveguide bend in Figure 1B [12, 21]. It consists of trapezoidal silicon segments aligned periodically along a 90° arc. The structure is equivalent to an inhomogeneous waveguide bend. The refractive index of the equivalent material can be calculated by the formula in (1) for parallel polarization, with f replaced by the radially varying duty cycle $\eta_0(R)$ [12, 21, 22]. Light propagating in the structure experiences a space-varying refractive index as in a gradient index (GRIN) fiber. With the help of transformation optics and geometrical optics, specific modal distributions and novel device functions can be attained by designing equivalent refractive index profiles in the waveguides.

When the geometry of the silicon segments changes from site to site on a 2D lattice with a subwavelength lattice constant, an equivalent metamaterial is formed. Figure 1C shows one such example. The silicon pillars

are distributed on a square lattice in a round area. The radius of the cylindrical pillar varies as a function of the distance between the position of the pillar and the center of the round area. The refractive index of the metamaterial can also be obtained using the formula in (1) for parallel polarization, with $f=\pi r(R)^2/\Lambda^2$ being the radius-dependent filling factor of the subwavelength pixel of the slab [13, 23, 24]. By varying the filling factor of each pixel, the equivalent refractive index can be engineered between those of silicon and the cladding material, providing the degree of freedom for better control of the polarization, mode, spatial distribution, and so on.

With the improvement of high-resolution lithography techniques, structures with feature sizes of ~100 nm can be routinely fabricated on the SOI platform. In Figure 2, we illustrate the fabrication process of the subwavelength structured silicon devices, which is widely used in the silicon photonics field. It starts with an SOI wafer, which has a 220-nm-thick silicon layer on top, a 3-μm-thick buried oxide layer in the middle, and a silicon substrate. Then EBL can be used to define the subwavelength structures and grating couplers on the photoresist, followed by the inductively coupled plasma (ICP) dry etching to transfer the pattern onto the silicon wafer. After obtaining the partially etched subwavelength structures and grating couplers, the EBL and ICP etching procedures are repeated to form the fully etched silicon waveguides. Finally, plasma enhanced chemical vapor deposition (PECVD) is used to deposit a 2-μm-thick layer of silica on the whole wafer. The silica fills in the gap between the silicon segments. In this way, one can fabricate a silicon subwavelength structured waveguide embedded in the silica cladding material with CMOS-compatible processing. This has motivated intense research efforts toward subwavelength structured devices. A variety of devices with unprecedented performance have been demonstrated based on different design principles. Among them, subwavelength structured polarization handling devices, mode manipulation devices, and optical interconnecting devices are the key components that have been extensively studied and used in integrated optical communication systems. In the following, we introduce the recent development of these three kinds of devices to illustrate how subwavelength structures can improve the performance of traditional silicon photonic devices.

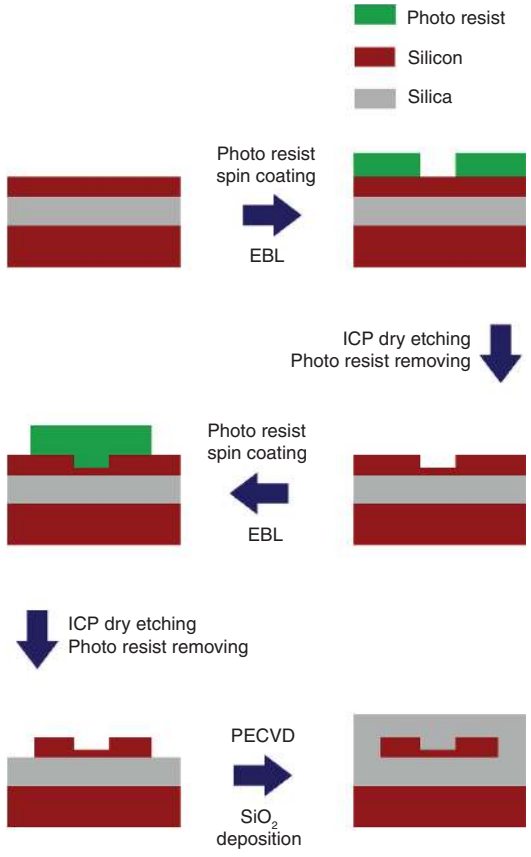

Figure 2: Schematic diagram of the fabrication process of subwavelength structured silicon devices.

3 Subwavelength structured polarization handling devices

The high index contrast and aspect ratio of the SOI waveguides result in large modal birefringence and therefore polarization mode dispersion and polarization-dependent loss, which hinder their applications in optical communications. To address this issue, polarization beam splitters (PBSs), polarization rotators (PRs), polarization beam splitters and rotators (PSRs), and on-chip polarizers are widely used in a polarization diversity scheme [25]. Subwavelength structured waveguides exhibit unique properties, such as strong anisotropy in the effective refractive index, which results in large modal birefringence for different polarizations. The waveguide birefringence can be utilized to realize polarization-dependent integrated devices.

3.1 Polarization beam splitters

In Qiu et al. [26], a compact PBS based on a grating-assisted coupler was numerically studied. The device configuration is shown in Figure 3A. By properly designing the waveguide width and the grating period, the injected transverse electric (TE) mode is contra–directionally coupled to waveguide *B* and reflected back

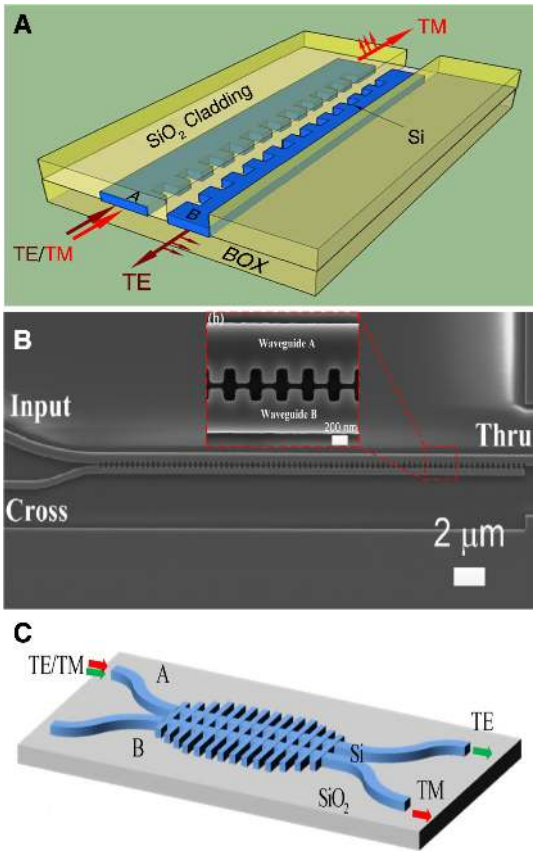

Figure 3: Schematic diagrams of the subwavelength structured PBSs.
(A) Grating-assisted contra-DC–based PBS. Reprinted from Qiu et al. [26]. Copyright © 2015 by the Optical Society of America. (B) Scanning electron microscopy image of the contra-DC–based PBS. Reprinted from Zhang et al. [27]. Copyright © 2016 by the Optical Society of America. (C) DC structure with grating perturbations. Reprinted from Liu et al. [28]. Copyright © 2016 by the Optical Society of America.

when the phase-matching condition is satisfied, whereas the transverse magnetic (TM)–polarized light is well confined within waveguide *A* and propagates through without coupling. Compared with conventional PBSs based on asymmetric directional couplers (DCs), this subwavelength structured PBS has a compact footprint (19 μm) and good fabrication tolerance to variations in the waveguide width (±40 nm). Fabrication and measurement of this grating-assisted PBS were carried out in Zhang et al. [27] (Figure 3B). A polarization extinction ratio (ER) over 30 dB was demonstrated with a ±10-nm tolerance to variations in the waveguide width. However, the operation bandwidth of this contra-DC structure is limited (~30 nm) due to the Bragg grating bandgap. To obtain a PBS with a broader bandwidth, a DC design with a subwavelength structured perturbation was introduced [28], as shown in Figure 3C. With the assistance of the subwavelength structured grating, a PBS was realized with a high ER of 24.8 dB and a broad bandwidth of 200 nm. However, an experimental demonstration of this design has not yet been reported.

To further reduce the device footprint, a compact subwavelength structured PBS was proposed with a coupling length of 6.8 μm in Xu and Xiao [29]. The schematic and simulated electric field distributions for TE and TM polarizations are shown in Figure 4A–C, respectively. An insertion loss (IL) of 0.08 dB (0.36 dB) and an ER of 32.19 dB (20.93 dB) for the TE (TM) mode were theoretically predicted. A similar design can be found in Zhang et al. [30]. To minimize the device size, a silicon nitride (SiN) layer on top of the SOI platform was introduced in Guo and Xiao [31], where the coupling length was only 2.7 μm.

Recently, a novel PBS based on heteroanisotropic metamaterial structures was proposed and experimentally demonstrated (Figure 5A) [32]. The SWG anisotropic

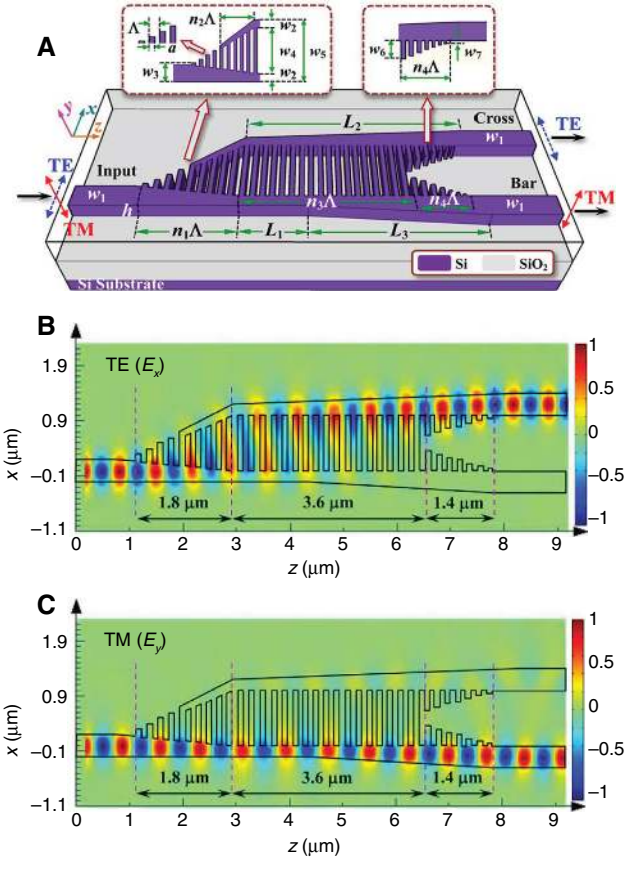

Figure 4: Theoretical study of an SWG-assisted PBS.
(A) Schematic diagram of the PBS. Simulated electric field distributions for (B) TE mode and (C) TM mode inputs. Reprinted from Xu and Xiao [29]. Copyright © 2016 by the Optical Society of America.

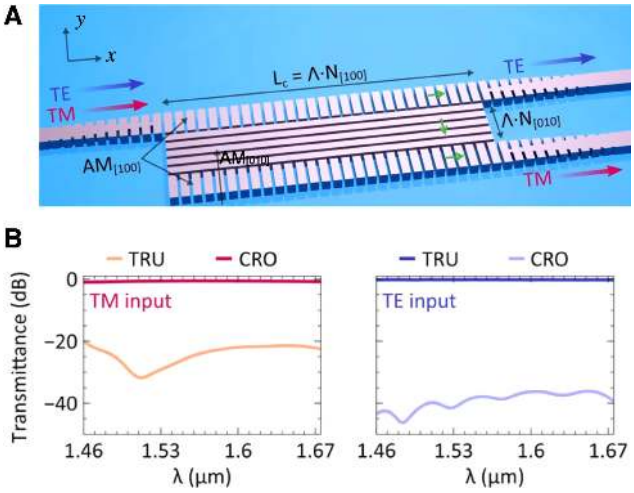

Figure 5: Ultrabroadband PBS using heteroanisotropic metamaterials.
(A) Schematic diagram of the PBS. (B) Simulated transmission spectra of the through and cross ports for TM and TE mode inputs. Reprinted from Xu et al. [32]. Copyright © 2019 by John Wiley and Sons.

metamaterial with an optical axis parallel to the x (y) direction is denoted as $AM_{[100]}$ ($AM_{[010]}$). The diagonal refractive index tensors for $AM_{[100]}$ and $AM_{[010]}$ metamaterials can be written as

$$n_{[100]} = \mathrm{diag}[n_{\perp}, n_{\parallel}, n_{\parallel}], \; n_{[010]} = \mathrm{diag}[n_{\parallel}, n_{\perp}, n_{\parallel}], \tag{2}$$

where $n_{\perp}$ and $n_{\parallel}$ can be calculated using (1). Therefore, the $AM_{[010]}$ section between two $AM_{[100]}$ SWG waveguides acts as an anisotropic slab. For TM-polarized light, it acts as a multimode interference (MMI) coupler, and the light is coupled to the cross port, whereas for TE-polarized light, it acts as a blocker, and the light will propagate directly to the through port without coupling. Attributed to the anomalous dispersion of the TE and TM modes in the subwavelength structured waveguides, a high ER of 20 dB and an ultrabroad working bandwidth of 200 nm can be achieved at the same time (Figure 5B).

3.2 Polarization rotators

After the splitting of the two polarization states, it is necessary to design a PR to convert one polarization to achieve the symmetrical configuration in the polarization diversity scheme. As the two polarizations are orthogonal, the vertical symmetry of the refractive index should be broken to increase the mode overlap between the two polarization states and hence enable efficient polarization conversion. The subwavelength structured waveguide is a good choice because of its flexible refractive index tuning property. In Wu and Xiao [33], a compact and broadband PR based on cross-slot waveguides was numerically investigated, where the rotation region of the PR was formed by subwavelength structured waveguides as shown in Figure 6A. The vertical refractive index symmetry is easily broken by the presence of gratings, leading to a hybrid mode profile at the cross section for the TE and TM polarizations. Thus, high-efficiency polarization rotation can be observed with a low IL (0.71 dB) and a broad bandwidth (260 nm). To simplify the fabrication process, a PR with subwavelength structured shallow-etched trenches was numerically studied in Xu and Shi [34], as shown in Figure 6B. The injected TM mode can be decomposed into a couple of hybridized modes (HP_1 and HP_2) with a 50:50 power coupling ratio. After the beat-length propagation in the cut-cornered waveguide, the TM mode is converted to the TE mode. The working bandwidth covers the O-, E-, S-, C-, L-, and U-band (1.26–1.675 μm). However, these PR designs are relatively difficult to fabricate, as at least a two-step etching process is required for each device. Accurate control over etching depth and precise layer alignment are challenging.

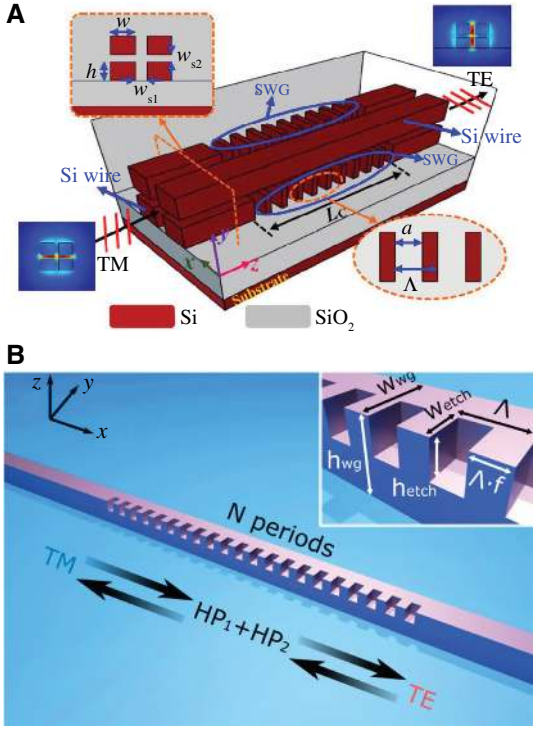

Figure 6: Schematic diagrams of the subwavelength structured PRs.
(A) Cross-slot waveguide-based PR. Reprinted from Wu and Xiao [33]. Copyright © 2017 by the Optical Society of America. (B) Subwavelength grating–assisted PR. Reprinted from Xu and Shi [34]. Copyright © 2019 by John Wiley and Sons.

3.3 Polarization beam splitters and rotators

A PSR combines the functions of a PBS and a PR and is capable of separating the two polarizations and simultaneously converting one of the polarizations to the other. It has attracted much attention as a promising polarization management device with a compact footprint. A subwavelength structured PSR was proposed in Xiong et al. [35], with its schematic configuration shown in Figure 7A. The effective index of the Bloch mode in the SWG waveguide is very close to that of the TM mode in the strip waveguide and differs significantly from that of the TE mode. Consequently, the TM mode launched from the left port can be successfully coupled to the SWG waveguide and converted to the TE mode in the transition taper connected to the cross port. In contrast, the injected TE mode fails to couple to the SWG waveguide due to the phase mismatch, so it propagates directly to the through port (Figure 7B). With the use of the subwavelength structured waveguide, the fabrication tolerance of the PSR is significantly improved. In He et al. [36], the PSR was experimentally demonstrated with a ±50-nm tolerance to variations in the waveguide width. Extinction ratios over 13 dB were achieved for both polarizations in the wavelength range from 1540 to 1580 nm. Fabrication tolerance in other dimensions, such as the gap and the duty cycle of the subwavelength structured waveguide, was further discussed in Wang et al. [37]. However, the bandwidth of this asymmetric DC-based PSR is intrinsically limited. To overcome this limitation, a partially etched subwavelength structured coupler was theoretically proposed in Xu and Xiao [38]. The injected TE mode is coupled to the adjacent partially etched waveguide gradually with the assistance of the subwavelength structured waveguide. Because of the vertical asymmetry induced by the shallow etched region, the TE mode is converted to the output TM mode simultaneously, whereas the launched TM mode is output from the through port with negligible coupling. The bandwidth can be increased to 102 nm while maintaining a high ER >20 dB.

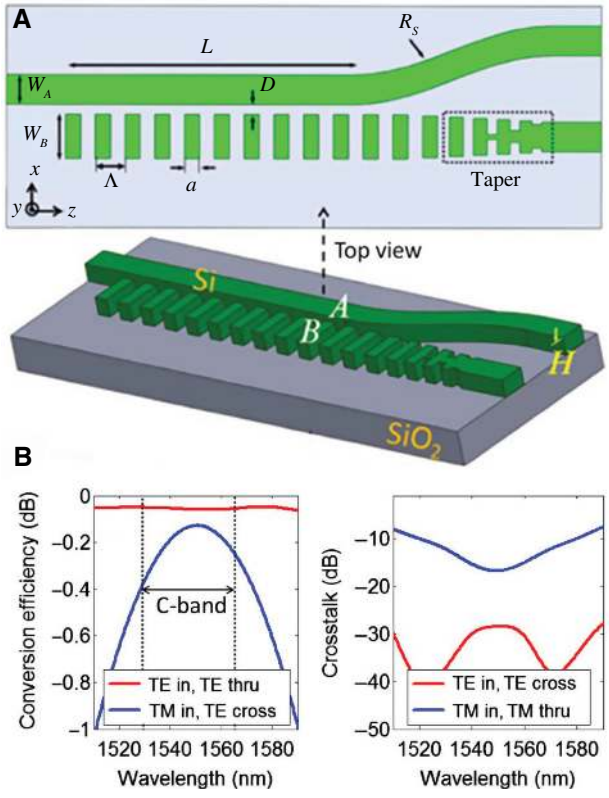

Figure 7: Theoretical study of a subwavelength structured PSR based on an asymmetric DC.
(A) Schematic diagram of the subwavelength structured PSR.
(B) Simulated wavelength dependence of the conversion loss and the CT. Reprinted from Xiong et al. [35]. Copyright © 2014 by the Optical Society of America.

3.4 Polarizers

Various polarization handling devices such as PBSs, PRs, and PSRs have been proposed for on-chip polarization management. However, the polarization ERs are typically insufficient. On-chip polarizers, which are capable of blocking one polarization while keeping the other one intact, are attractive for enhancing the polarization ERs. In Guan et al. [39], a TM-pass polarizer was proposed and experimentally demonstrated. A scanning electron microscopy image of the fabricated devices is shown in Figure 8A. The subwavelength structured waveguide is designed to support the Bloch mode for TM polarization only, while it acts as a Bragg grating reflector for the TE mode by properly choosing the period of the grating structure. The polarization ER is greater than 40 dB in the wavelength range from 1520 to 1560 nm. Similar designs have also been proposed to realize a TM polarizer [41] and a TE polarizer [42]. In Shahin et al. [41], the TE mode is radiated out to avoid damage to the laser source caused by the reflected light. In Xiong et al. [42], the period of the grating was designed such that the device works under the cutoff condition for the TM mode with an ER of ~30 dB. The TE mode propagates with an IL of 0.4 dB in the wavelength range from 1470 to 1580 nm. Recently, an anisotropic metamaterial-assisted on-chip all-silicon polarizer with an extremely broad working bandwidth was proposed and experimentally demonstrated (Figure 8B) [40]. The device is based on

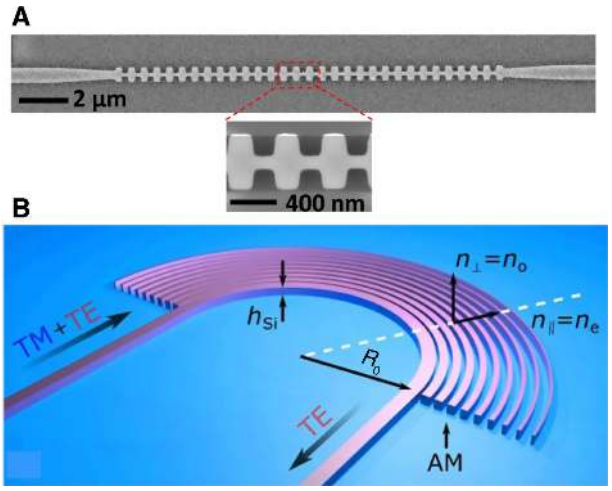

Figure 8: Schematic diagrams of the subwavelength structure–based polarizers.
(A) Basic subwavelength structured waveguide TM polarizer design. Reprinted from Guan et al. [39]. Copyright © 2014 by the Optical Society of America. (B) Ultrabroadband TE polarizer using an anisotropic metamaterial. Reprinted from Xu et al. [40]. Copyright © 2019 by Chinese Laser Press.

a 180° sharp waveguide bend, assisted with anisotropic SWG metamaterial cladding to enhance the polarization selectivity. For the TE polarization, the SWG effective refractive index is extraordinary, which is much smaller than the silicon refractive index. The incident TE mode can be tightly confined and can propagate through the sharp waveguide bend with negligible bending loss. For the TM polarization, the SWG effective refractive index is ordinary, which is quite close to the silicon refractive index. The incident TM mode will be weakly confined and coupled into the radiation mode regardless of the wavelength; that is, it will be efficiently filtered out. The fabricated polarizer shows low loss (<1 dB) and a high polarization ER (>20 dB) over a bandwidth of >415 nm from 1.26 to 1.675 μm.

The experimental results for the abovementioned subwavelength structured polarization handling devices are summarized in Table 1.

4 Subwavelength structured mode handling devices

Mode handling devices are key components in on-chip mode division multiplexing systems. As mode coupling and conversion depend on the propagation constant difference of two modes $\beta_1 - \beta_2$, $d\beta_1/d\lambda = d\beta_2/d\lambda$ should be satisfied to obtain an ultrabroad bandwidth. Similarly, $d\beta_1/dw = d\beta_2/dw$ is required to achieve fabrication tolerance with respect to the geometrical parameter w. It is difficult to meet these two conditions in conventional SOI waveguides. However, benefiting from the tunability of the effective index and the ability of mode dispersion engineering, both $\beta_1 = \beta_2$ and $d\beta_1/d\lambda = d\beta_2/d\lambda$ ($d\beta_1/dw = d\beta_2/dw$) can be satisfied in subwavelength structured waveguides. Consequently, subwavelength structured mode handling devices are more tolerant to wavelength variations and fabrication errors than their silicon waveguide counterparts [9].

Figure 9A shows a high-order mode (de)multiplexer that consists of an SWG waveguide coupled to a strip bus waveguide. Using an eigen mode solver, one can calculate the effective index of the Bloch mode in the access SWG waveguide and that of the TE_6 mode in the silicon bus waveguide as a function of the waveguide width (Figure 9B). Phase matching between these two modes can be achieved by carefully choosing the waveguide widths, for example, the circled points in Figure 9B. The slopes at these two points are very close to each other, which means that the mode coupling is robust to the waveguide width variation. As a result, high-efficiency coupling will occur between these two waveguides, accomplishing the mode conversion from the TE_0 mode at the input port to the TE_6 mode at the output port (with the help of the strip-to-SWG transition taper). In addition, it is quite tolerant to fabrication error in the waveguide width. Based on this technique, a high-efficiency three-mode (de)multiplexer was built with SWG DCs, showing CT values of <–16.3 dB and ILs of <3.8 dB at 1550 nm [43]. Thanks to the fabrication tolerance and therefore the scalability of the SWG DCs, the

Table 1: Performance of some subwavelength structured polarization handling devices.

Structure and reference	IL (dB)	ER (dB)	Bandwidth (nm)	Device length (μm)
Grating-assisted contra-DC PBS [27]	<1	>30	20	27.52
Hetero-anisotropic metamaterial structure [32]	<1	>20	>200	12.25
SWG-based DC PSR with a TM filter [36]	1.5	~13	73	<45
SWG-based DC PSR [37]	1.3	10	50	35
SWG-bridged polarizer [39]	0.5	20	60	~9

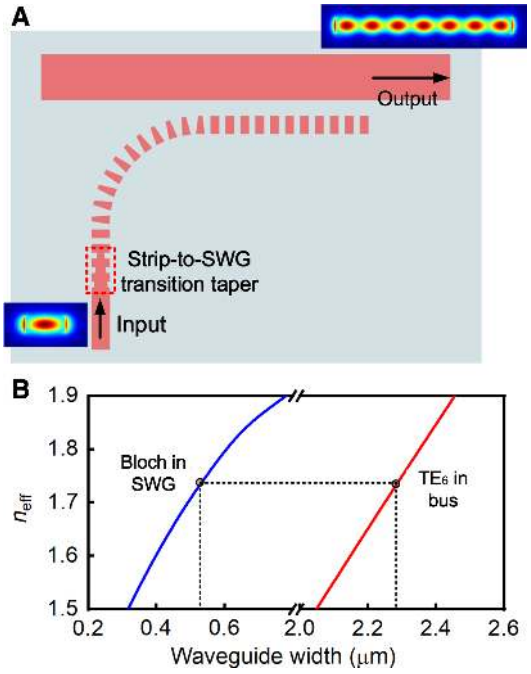

Figure 9: High-order mode (de)multiplexer employing SWG waveguides.
(A) Schematic diagram of the (de)multiplexer structure. (B) Effective indices of the TE_6 mode in the strip waveguide and the Bloch mode in the SWG waveguide as a function of the waveguide width. The waveguide widths used in the (de)multiplexer are indicated by circles in the figure. The structure in A was reported in He et al. [43].

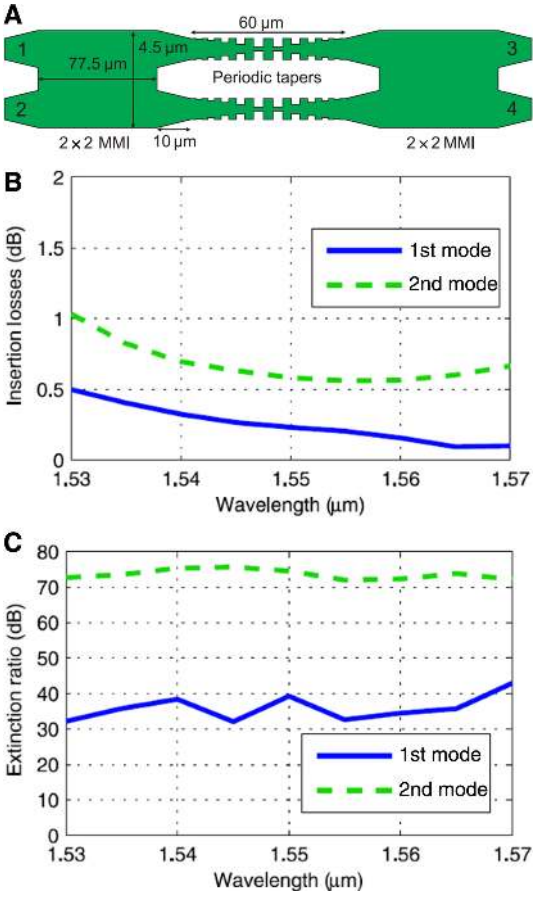

Figure 10: Theoretical study of an add/drop mode multiplexer.
(A) Schematic diagram of the mode multiplexer based on MMIs and an MZI coupler with SWG waveguides in both arms. Simulated device performance of the (B) IL and (C) ER as a function of wavelength. Reprinted from Pérez-Galacho et al. [47]. Copyright © 2015 by the IEEE.

design was later extended to an 11-mode (de)multiplexing (TE_0–TE_{10}) device [44]. Low CT values (–15.4 to –26.4 dB) and ILs (0.1–2.6 dB) were measured for all 11 channels at 1545 nm. To further broaden the working bandwidth, the adiabatic coupling technique is also introduced in the SWG-based (de)multiplexer. The Allen–Eberly coupler was constructed using the SWG to realize a TE_0-to-TE_{12} mode-order converter with the conversion efficiency better than –1.5 dB over a 75-nm bandwidth [45]. A two-mode (de) multiplexer employing the SWG adiabatic coupler was predicted by simulations to have a bandwidth of 740 nm spanning from 1260 to 2000 nm, where the CT was lower than –18.5 dB, and the IL was better than 0.32 dB [46]. In the experiment, a CT of <–18.8 dB and an IL of <2.6 dB were measured over an ultrabroad bandwidth covering the O-, C-, and L-band.

Other devices, such as the Mach–Zehnder interferometer (MZI) and MMI coupler, can also be implemented using subwavelength structures. An add/drop mode multiplexer was constructed based on an MZI with SWG waveguides in both arms (Figure 10A) [47–49]. The principle of operation is as follows: the TE_0 and TE_1 modes are launched into the device through port 1 and split by the input MMI coupler. The TE_0 mode is reflected in the SWG waveguides and outputs at port 2; the TE_1 mode propagates through the SWG waveguides and outputs at port 4 of the output MMI coupler. Another TE_0 (TE_1) mode signal can be added from port 3 and combined with the TE_1 (TE_0) mode in port 4 (port 2). Simulation results indicate that the device has an IL of <1 dB and an ER of >30 dB in the whole C-band (Figure 10B, C). An ultrabroadband two-mode multiplexer using the SWG MMI coupler was designed based on the beam shaping technique (Figure 11A) [50–52]. The TE_0 mode input from port 1 (port 2) is distributed to the two output ports of the MMI coupler. The upper branch has a 90° phase advance (delay) compared to the lower branch. A –90° phase shifter is cascaded to the upper branch to obtain the in-phase (out-of-phase) TE_0 modes in the branching waveguides. The desired TE_0 (TE_1) mode profile can be formed at the joint of the two branches where the two beams in

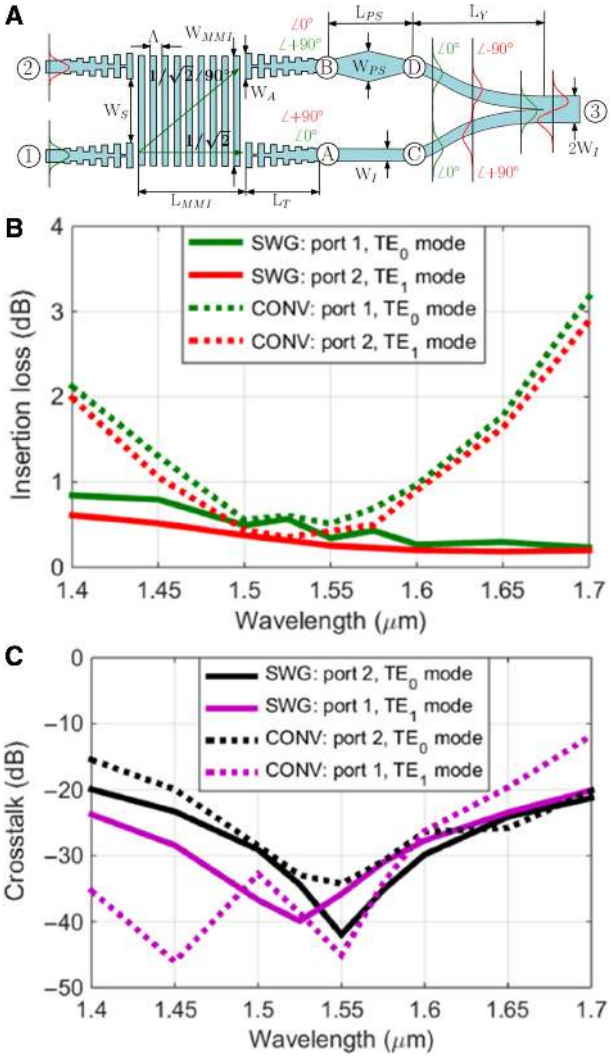

Figure 11: Theoretical study of an ultrabroadband mode multiplexer. (A) Schematic diagram of the mode multiplexer based on SWG MMI, a –90° phase shifter and a Y junction. Simulated device performance of the (B) IL and (C) CT as a function of wavelength. Reprinted from González-Andrade et al. [50]. Copyright © 2018 by the IEEE.

the separate branches are combined. A theoretical study proved that the device exhibits an IL of <0.84 dB and a CT value of <– 20 dB over an ultrabroad bandwidth of 300 nm (1.4–1.7 μm) (Figure 11B, C).

A refractive index perturbation can be introduced by metasurface structures to assist the mode-order conversion between two specific modes in dielectric waveguides. The conversion between two modes can be described by the following mode coupling equations [53]:

$$-\frac{\partial A}{\partial z} = i\kappa_{ab} B e^{i(\beta_a - \beta_b)z},$$
$$-\frac{\partial B}{\partial z} = i\kappa_{ba} A e^{i(\beta_b - \beta_a)z}, \quad (3)$$

where A and B are the amplitudes of waveguide modes a and b, respectively; β_a and β_b are the propagation constants of the two modes; and κ_{ab} and κ_{ba} represent the exchange coupling coefficients between modes a and b. Etching patterns can be designed using the EMT to realize various mode-order converters in silicon waveguides [54]. A TE_0-to-TE_1 mode converter was experimentally demonstrated in an SOI waveguide with a high mode purity and a relatively low IL (Figure 12A) [55]. Gradient metasurface structures consisting of phased arrays of plasmonic or dielectric nanoantennas were applied at subwavelength intervals to realize waveguide mode converters on silicon, SiN, and lithium niobate platforms (Figure 12B) [56]. TE_0-to-TE_1 and TE_0-to-TE_2 mode converters were experimentally implemented using all-dielectric metasurface structures with tilted subwavelength slots (Figure 13A) [57]. Figure 13B and C display the measured transmission spectrum of each mode in the fabricated TE_0-to-TE_1 and TE_0-to-TE_2 mode-order converters, respectively. For the TE_0-to-TE_1 mode converter, the conversion loss is lower than 1 dB, and the CT value is below –10 dB in the wavelength range of 1542–1563 nm. For the TE_0-to-TE_2 mode converter, a conversion loss of <0.5 dB and a CT value of <–10 dB are achieved in the wavelength range of 1545–1565 nm. The coupling lengths are 5.75 and 6.736 μm for the TE_0-to-TE_1 and TE_0-to-TE_2 mode conversions, respectively.

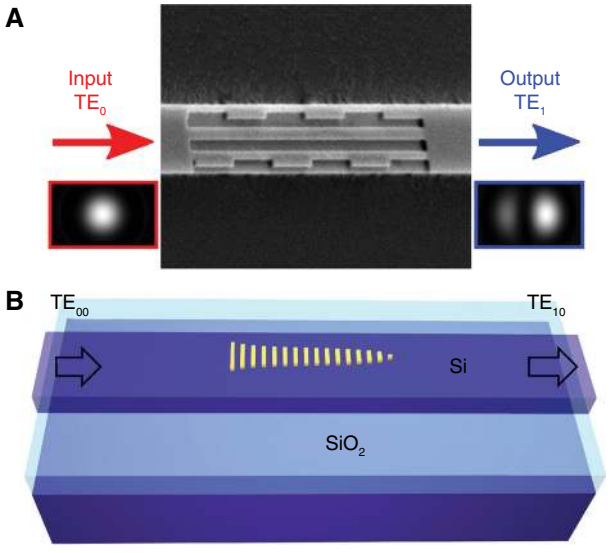

Figure 12: Schematic diagrams of waveguide mode converters assisted by metasurface/subwavelength structures. TE_0-to-TE_1 mode converter with a (A) subwavelength feature and (B) metasurface consisting of gold nanoantennas. The golden color represents gold. A is reprinted from Ohana et al. [55]. Copyright © 2016 by the American Chemical Society. Figure B is reprinted from Li et al. [56]. Copyright © 2017 by Springer Nature.

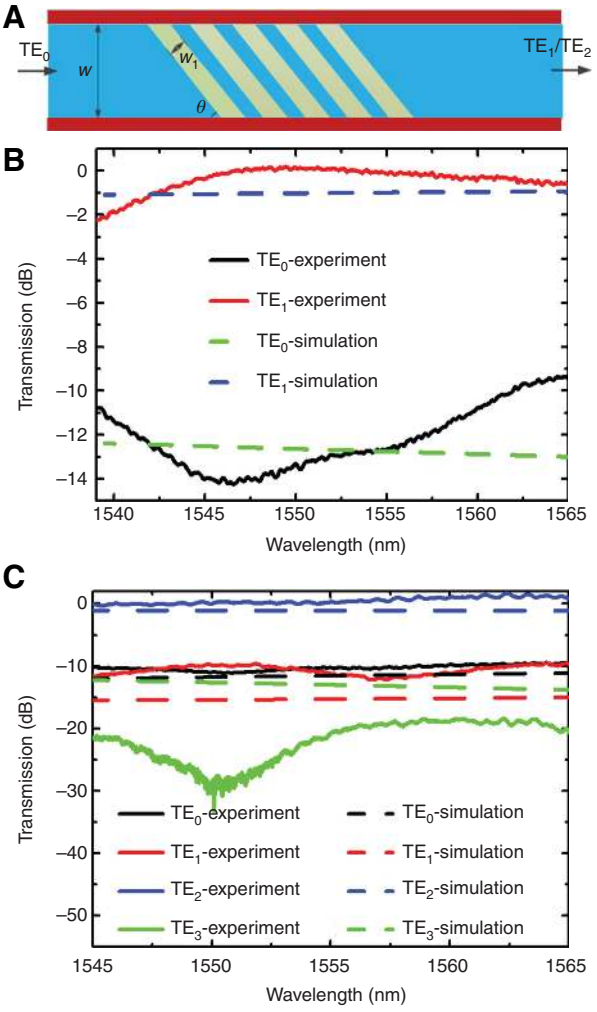

Figure 13: Experimental demonstration of a mode-order converter with tilted subwavelength slots.
(A) Schematic diagram of the mode-order converter. The blue, yellow, and dark red colors represent silicon, partially etched silicon, and silica, respectively. Measured transmission spectra of (B) a fabricated TE_0-to-TE_1 mode converter and (C) a fabricated TE_0-to-TE_2 mode converter compared with simulation results. Reprinted from Wang et al. [57]. Copyright © 2019 by John Wiley and Sons.

Similar structures were proposed to realize TE_0-to-TE_1, TE_0-to-TE_2, and TE_0-to-TE_3 mode-order converters [58]. Numerical results show that the conversion efficiencies of TE_0-to-TE_1, TE_0-to-TE_2, and TE_0-to-TE_3 mode-order converters are larger than 94.4%, 95.7%, and 83.7% in the wavelength range from 1.5 to 1.6 μm, with corresponding device lengths of 8.72, 4.98, and 14.54 μm, respectively. Recently, TE_1-to-TE_2 mode conversion was achieved via two cascaded SWGs, which shows the potential for realizing arbitrary mode-order converters by cascading multiple SWGs [59].

Another type of mode handling device is the mode blocking filter, which suppresses undesired modes without affecting others. TE_0 and TE_1 mode blockers based on SWG contra-DCs were demonstrated with CT values of <–21 dB and ILs of <2.3 dB [60]. A TM_1 mode pass filter employing cascaded plasmonic bridged SWGs was theoretically investigated [61]. Simulation results showed that an IL of 0.63 dB, a 3-dB bandwidth of 493 nm (1.222–1.715 μm), and a mode ER of 26.4 dB can be achieved in the proposed structure.

Subwavelength structured mode handling devices with state-of-the-art performances are summarized in Table 2. Employing adiabaticity and subwavelength structures simultaneously in the design shows potential for broadening the working bandwidth while shortening the device length.

5 Subwavelength structured building blocks for optical interconnects

Waveguide couplers, splitters, crossings, and waveguide bends are essential building blocks in on-chip optical interconnect systems [62]. Grating couplers and edge couples are basic elements that couple light from silicon waveguides to optical fibers, serving as fiber-chip interconnects. Subwavelength structures have been employed in these devices. In the following, some results for these kinds of devices based on subwavelength structures are reviewed.

Table 2: Experimental results for various subwavelength structured mode multiplexers and converters.

Structure and reference	IL (dB)	CT (dB)	Footprint (μm²)	Bandwidth (nm)
Mode (de)multiplexer based on an SWG [44]	<2.3	<–19.8	4.2×5	50
Adiabatic DC based on an SWG [45]	<1.5	–	5×75	75
Adiabatic coupler based on an SWG slot [46]	<2.6	<–18.8	2.45×55	740
Dielectric metasurface waveguide [55]	0.55	–13	1×23	–
Waveguide with a metasurface [57]	<1	<–10	1.4×6.736	20
TE_0 (TE_1) mode blocker [60]	<1.4 (<2.3)	<–21 (<–25.6)	1.9×10 (2.2×20)	35 (26)

5.1 Couplers and splitters

Waveguide couplers and splitters are used to combine and split two beams of light. Many types of couplers and splitters have been demonstrated on the SOI platform using different structures, such as a DC [63], an MMI coupler [64], and a Y junction [65]. Superimposing a subwavelength structure on conventional waveguides provides an approach to tailor the dispersions of the supermodes and improve the performances of the devices [66]. The following section reviews some recent results for waveguide couplers and splitters with four typical subwavelength structures, as shown in Figure 14.

Directional couplers are widely used in on-chip silicon couplers and splitters because the power splitting ratio in two parallel waveguides can be controlled by the coupling strength and/or the coupling length. However, wavelength variations lead to deviations in both the effective indices and the coupling strengths; thus, the working bandwidth is limited. By adopting SWG structures in the DC architecture, a fivefold broader bandwidth was theoretically achieved compared to traditional DCs [67]. Then, DCs with SWG structures were experimentally demonstrated with a bandwidth of 100 nm for power splitting ratios of 50/50, 40/60, 30/70, and 20/80 [70]. A DC consisting of two tapered SWG waveguides was used to achieve an adiabatic mode evolution for broadband 3-dB power splitting with a coupling length of 50 μm [68]. Excess losses of <0.5 dB and an imbalance of <0.3 dB were obtained over a 130-nm bandwidth. Recently, an adiabatic 3-dB coupler based on an SWG slot structure was demonstrated with a mode-evolution length of only 25 μm, an average IL of 0.2 dB, and a power splitting ratio better than 3 ± 0.27 dB over a 100-nm bandwidth [71]. By properly designing the subwavelength structure in the directional coupling region, the coupling strength for TE polarization can be tuned to be very close to that for TM polarization, leading to similar coupling lengths for both polarizations. Based on this concept, an ultracompact polarization-independent DC employing subwavelength "nanoteeth" on the waveguides was demonstrated with a coupling length of 3.75 μm [72].

Multimode interference couplers based on the self-imaging effect are used in a wide variety of waveguide devices [73]. The lengths and performances of MMI couplers depend on the beat length of the two lowest-order modes in the multimode region. Typically, the bandwidth is limited to ~100 nm for a 2×2 MMI with an IL of 1 dB. The dispersion property of the multimode region can be engineered using an SWG structure to mitigate the wavelength dependence of the device [74]. A measured bandwidth of 300 nm was achieved in a 2×2 MMI coupler with an SWG multimode waveguide [69]. The

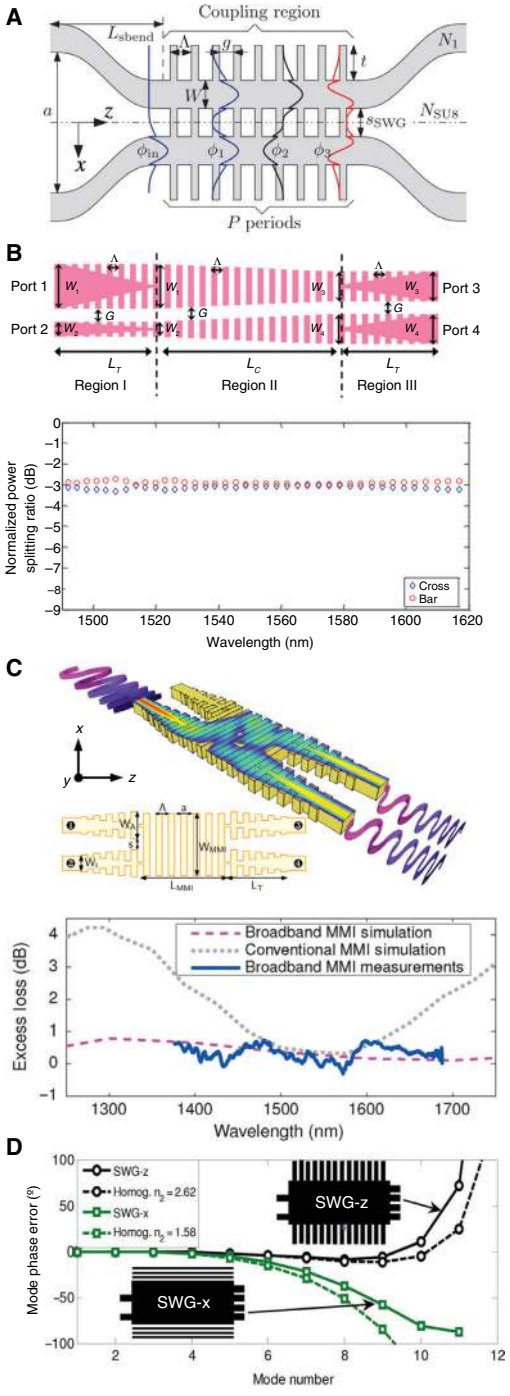

Figure 14: Results for various subwavelength structured couplers and splitters.
(A) Theoretical study of a DC with subwavelength structures. Reprinted from Halir et al. [67]. Copyright © 2012 by the Optical Society of America. (B) Experimental demonstration of a DC consisting of two SWG waveguides. Reprinted from Yun et al. [68]. Copyright © 2016 by the Optical Society of America. (C) Experimental demonstration of a 2×2 MMI based on an SWG multimode waveguide. Reprinted from Halir et al. [69]. Copyright © 2016 by John Wiley and Sons. (D) Theoretical study of a 2×4 MMI with subwavelength lateral claddings. Reprinted from Ortega-Monux et al. [64]. Copyright © 2011 by the IEEE.

length is approximately half that of a traditional 2×2 MMI. With the advantages of fully passive structure and high fabrication tolerance, 2×4 MMI couplers are preferred as optical 90° hybrids, which are essential components in optical coherent receivers [75]. The performance of a conventional 2×4 MMI is limited by the high lateral refractive index contrast. By using subwavelength structures in the lateral cladding regions, the bandwidth of the subwavelength structured 2×4 MMI is extended from 36 to 60 nm, compared to that of a conventional 2×4 MMI [64]. An SWG structure can also be used as the multimode region of a 2×4 MMI to increase the bandwidth. Recently, a 2×4 MMI coupler with an SWG multimode waveguide was theoretically studied, which had a length of 41.3 μm and a bandwidth of >150 nm [76]. The experimental results for some silicon subwavelength structured couplers and splitters are summarized in Table 3.

5.2 Waveguide crossings

On-chip integrated photonic circuits require efficient waveguide crossings to facilitate connectivity and minimize the device footprint. A conventional waveguide intersecting with another one creates a region with no lateral mode confinement, leading to high loss and considerable CT. Low-loss and low-CT waveguide crossings can be implemented by subwavelength structures, such as SWG [77], Maxwell's fisheye lens [78], and so on.

When two SWG waveguides intersect with each other, both the loss and the CT can be reduced on account of the propagating Bloch modes. An SWG waveguide crossing was reported with a loss of 0.023 dB/crossing, a polarization-dependent loss of <0.02 dB, and a CT value of <–40 dB [77]. Subwavelength nanostructures were used as the lateral cladding of MMI crossings to achieve low index contrast and reduce the ILs. A 101×101 MMI crossing array with subwavelength lateral claddings was fabricated with a pitch of 3.08 μm. The measured results showed that the loss was ~0.02 dB/crossing, and the CT was <–40 dB [79].

Spatially inhomogeneous metamaterials can be realized in silicon slab waveguides by controlling the effective material refractive indices with subwavelength structures. Combined with transformation optics (especially conformal mapping [80] and quasi-conformal mapping methods [78]) and geometrical optics, it offers a large degree of freedom to manipulate the propagation of light in a silicon chip and implement new device functions. The demonstrated subwavelength metamaterial devices include invisible cloaks [81], spot size converters [82], Maxwell's fisheye [83] and Luneburg lenses [24], dual-function "Janus" devices [84], and so on. For example, it is well known in geometrical optics that Maxwell's fisheye lens can focus rays emanating from a point on the boundary of the lens to a conjugate point on the opposite side [85]. This unique property can be utilized to realize a waveguide crossing for up to eight waveguides with a loss of 0.1 dB and a CT value of −40 dB in simulations [86]. Experimentally, Maxwell's fisheye lens can be built on a silicon slab by designing the geometry of the silicon pillars shown in Figure 1C. A silicon eight-port multimode waveguide star crossing was experimentally demonstrated to support the propagation of TM_0 and TM_1 modes. Figure 15A shows how the incident TM_1 mode propagates through the waveguide crossing. Thanks to the self-imaging property, it forms the same mode profile at the other end of the lens, making the intermodal CT low enough for a multimode crossing (Figure 15B). The measured results show that the losses are <0.3 dB and the CT values are <–20 dB [13]. More recently, a universal multimode waveguide star crossing supporting an arbitrary number of waveguide modes and crossing channels was proposed and demonstrated based on Maxwell's fisheye lens [83]. The device was fabricated by gray-scale EBL. A 3×3 silicon slot waveguide crossing was also theoretically proposed based on Maxwell's fisheye lens [87]. Some of the subwavelength structured waveguide crossings are listed in Table 4.

5.3 Waveguide bends

Benefitting from the high index contrast of silicon waveguides, ultrasharp single-mode waveguide bends with

Table 3: Experimental results for subwavelength structured couplers and splitters.

Structure and reference	Loss (dB)	Imbalance (dB)	Footprint (μm²)	Bandwidth (nm)
2×2 DC with SWGs [70]	–	0.7	3×14	100
DC with SWG waveguides [68]	0.5	0.3	1×50	130
2×2 SWG slot DC [71]	0.2	0.27	2×65	100
2×2 SWG MMI [69]	1	0.5	3.25×14	300

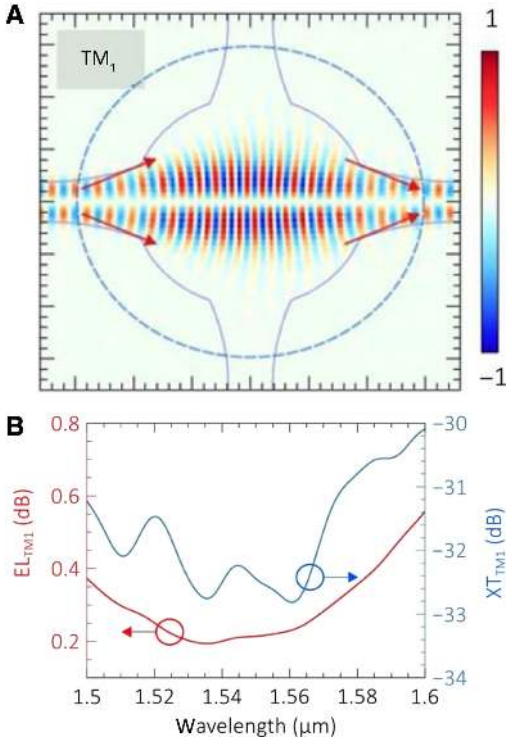

Figure 15: Multimode crossing using a subwavelength metamaterial-based Maxwell's fisheye lens.
(A) Field distribution of the TM_1 mode when crossing the subwavelength structured area. (B) Simulated excess loss and CT spectra for the TM_1 mode. Reprinted from Xu and Shi [13]. Copyright © 2018 by John Wiley and Sons.

radii of <2 μm have been reported, enabling large-scale photonic integration [88]. However, for a multimode waveguide bend, there is a significant mode mismatch between the straight waveguide and the bent section, leading to large mode-mismatching losses and intermodal CT. For a 4-μm-wide multimode waveguide, a bend radius of >1 mm is needed to minimize the mode mixing, which is unacceptably large for high-density photonic integration [89]. Subwavelength nanostructures can be used to achieve ultrasharp multimode waveguide bends. One approach is to introduce a mode converter with a subwavelength structured poly(methyl methacrylate) upper cladding between the straight multimode waveguide and the bent section so that the mode mismatch and intermode coupling can be significantly reduced. A sharp multimode waveguide bend with a 30-μm radius was demonstrated with a loss of <1 dB and a CT value of <–20 dB over a bandwidth of >80 nm [22]. Another method that can be used to achieve ultrasharp multimode waveguide bends is to tailor the index profile of the bent section. The refractive index near the inner arc of the bend is designed to be larger than that near the outer arc so that the mode in the inhomogeneous bend overlaps with that in the silicon strip waveguide to a large extent. As a consequence, the modes in the straight strip waveguide can pass through the 90° SWG bend with low IL and negligible intermodal CT. A subwavelength-resolution GRIN profile was introduced in the waveguide bend, which was designed by transformation optics and fabricated by gray-scale EBL. A 4-μm-wide multimode waveguide bend was demonstrated with a bending radius of 78.8 μm and a loss of 2.6 dB [89]. Recently, shallow-etched SWG structures have been introduced in the multimode bent section to modify the index profile and reduce the mode mismatch (Figure 1B). An ultrasharp 90° waveguide bend with a radius of 10 μm was demonstrated with an excess loss of <0.7 dB and a CT value of <–22 dB for three TE modes (TE_0–TE_2) in the wavelength range of 1520–1600 nm [12]. The design can also be extended to four-mode channels (TE_0–TE_3). Figure 16A shows how the TE_3 mode passes through the SWG multimode waveguide bend, whereas Figure 16B shows the transmission spectrum of each mode at the output end of the bend. An excess loss of <0.8 dB and a CT value of <–15 dB were measured with a bending radius of 20 μm over a 90-nm wavelength band (1520–1610 nm). Table 5 shows some of the recently reported subwavelength structured multimode waveguide bends.

5.4 SWG couplers for fiber-chip interconnects

Grating couplers and edge couples are frequently used to couple light from silicon waveguides to optical fibers for fiber-chip interconnects. Normally fiber-chip coupling is

Table 4: Experimental results for subwavelength structured waveguide crossings.

Structure and reference	Loss (dB/crossing)	CT (dB)	Footprint (μm²)
SWG waveguide crossing [77]	0.023	−40	<0.5×0.5
MMI crossing with subwavelength claddings [79]	0.02	−40	–
Maxwell's fisheye lens multimode crossing [13]	0.3	−20	18×18
Multimode waveguide star crossing [83]	<2.68	−19.5	42×42

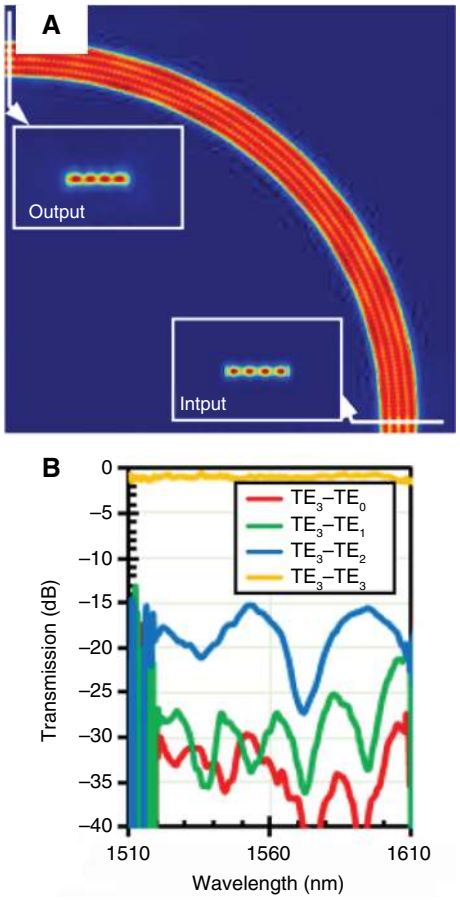

Figure 16: Experimental demonstration of an SWG multimode waveguide bend.
(A) Field distribution of the TE_3 mode when passing through the SWG waveguide bend. (B) Measured transmission spectra when the TE_3 mode is launched into the waveguide bend. Reprinted from Wu et al. [12]. Copyright © 2019 by John Wiley and Sons.

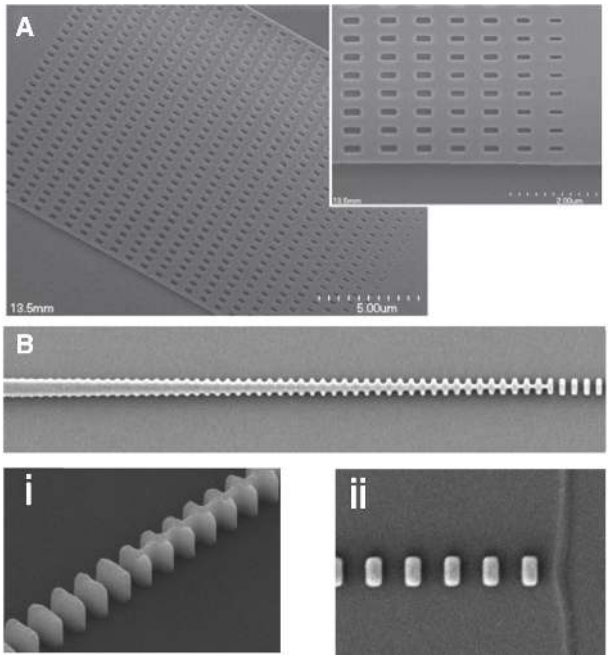

Figure 17: Experimental demonstration of SWG couplers for fiber-chip interconnects.
(A) Scanning electron microscopy image of the fabricated continuously apodized SWG surface grating coupler. Inset: detailed view. Reprinted from Benedikovic et al. [90]. Copyright © 2014 by John Wiley and Sons. (B) Scanning electron microscopy image of the SWG edge nanocoupler. Insets (i) and (ii) show the coupler tip and the intermediate section positioned at 15 μm from the junction with silicon wire waveguide, respectively. Reprinted from Cheben et al. [91]. Copyright © 2015 by the Optical Society of America.

challenging because of the large mode area (wavevector) mismatch between a silicon waveguide and an optical fiber. For vertical coupling, the wavevector mismatch can be compensated by a grating, whereas for the edge coupling, the mode area of a silicon waveguide can be expanded by using a subwavelength structure. In the following, we summarize some results on subwavelength structured grating couplers and edge couplers. A typical SWG surface grating coupler and a typical SWG edge coupler are shown in Figure 17.

Grating couplers attract much attention due to their advantages of easy wafer-scale testing and high tolerances for fiber alignment [92]. The key parameters of grating couplers include the coupling efficiency, bandwidth, large alignment tolerance, and so on [93]. High-efficiency single-etch grating couplers can be realized based on subwavelength structures (Figure 17A). Coupling losses of 2.16 dB at 1.55 μm [90] and 2.5 dB at 1.3 μm [94] have been experimentally demonstrated. L-shaped grating couplers were used to increase the directionality of the gratings. A measured coupling loss of 2.7 dB was achieved with a bandwidth of 62 nm [95]. Through the grating apodization, a high-efficiency bidirectional

Table 5: Experimental results for some subwavelength structured bends.

Structure and reference	Loss (dB)	CT (dB)	Radius (μm)	Bandwidth (nm)
Subwavelength structured upper-cladding bend [22]	<1	–20	30	>80
Transformation optic–based bend [89]	2.6	–	78.8	–
Shallow-etched SWG bend [12]	0.7	–22	10	80

Table 6: Experimental results for subwavelength structured fiber-to-chip grating couplers.

Structure and reference	λ (nm)	Coupling loss (dB)	1-dB BW (nm)	θ
Interleaved SWG structures [98]	1570	5.1	70	16
Single-etch subwavelength [90]	1550	2.16	~35	27
Focusing curved SWG [99]	1550	4.7	100	20
1D nonuniform grating [100]	1550	3.8	90	24.7
SWG with a backside metal reflector [97]	1538	0.69	~30	27
Single-etch SWG [94]	1310	2.5	40	–
L-shaped grating [95]	1550	2.7	62	22
HPF SWG [101]	1550	7.49	14	8
Apodized bidirectional grating [96]	1530	1.8	37	–

Table 7: Experimental results for subwavelength structured fiber-to-chip edge couplers.

Structure and reference	λ (nm)	Coupling loss (dB)	Minimum feature size (nm)	1-dB BW (nm)
SWG tip [102]	1530	0.9	100	–
Polarization-independent SWG [91]	1550	0.32	–	>100
SWG 12-fiber assembly [103]	1490	1.6	140	~100
V-groove SWG membrane [104]	1515	1.4	120	>200

grating coupler using SWGs could be realized with a coupling loss of 1.8 dB and a 1-dB bandwidth of 37 nm [96]. By adding a backside metal reflector, a subwavelength engineered grating coupler was demonstrated with a measured coupling loss of 0.69 dB and a 3-dB bandwidth of 60 nm [97]. Conventional grating couplers usually exhibit limited operation bandwidths. By interleaving dispersion engineered subwavelength structures, a 1-dB bandwidth of 70 nm and a 3-dB bandwidth of 117 nm could be achieved [98]. An ultrabroad 1-dB bandwidth of more than 100 nm was experimentally realized based on focusing-curved subwavelength structures [99]. Using 1D SWG structures, both straight and focusing grating couplers could be achieved with a 1-dB bandwidth of 90 nm [100]. Grating couplers with high alignment tolerance could also be realized based on SWG structures. An apodized single-etch–step SWG grating coupler was demonstrated with high lateral misalignment tolerance and a coupling loss of 7.49 dB [101]. Table 6 shows some of the recently reported subwavelength structured grating couplers.

Edge couplers can provide high coupling efficiency, ultrawide bandwidth, and polarization-independent operation [91]. Benefitting from the effective index modification effect, SWG waveguides can be used to expand the mode field in a silicon waveguide, which help maximize the overlap between the modes in the SWG waveguide and the lens fiber (Figure 17B) [5, 91]. An SWG-based edge coupler was demonstrated experimentally with coupling losses of 0.9 dB for TE polarization and 1.2 dB for TM polarization [102]. A metamaterial converter between standard fibers to nanophotonic waveguides was reported with both manual probing and a self-aligned 12-fiber automated assembly [103]. The peak transmission efficiency was –1.6 dB. Fiber V-grooves were integrated on the chip with metamaterial converters embedded in suspended oxide membranes to prevent coupler-mode leakage to the substrate. The coupler fabricated with a 300-mm CMOS production facility was demonstrated with a peak transmission of –0.7 dB for TE polarization and –1.4 dB for TM polarization [104]. Silicon nitride layers with SWG structures were introduced to reduce the leakage to the silicon substrate [105]. A coupling loss of 0.35 dB and a 1-dB bandwidth of 95 nm were reported in an SiN-assisted edge coupler [106]. Robust edge couplers are desired for high-volume production. An SWG-based edge coupler for coupling to high-numerical-aperture optical fibers was proposed theoretically with high tolerance to fiber misalignment (±1.5 μm for a 1-dB excess loss) [107]. Subwavelength grating mode converters are also used for optical chip-to-chip connections. Highly broadband coupling was demonstrated with a penalty of <0.35 dB over a 120-nm bandwidth [108]. Table 7 shows some of the recently reported subwavelength structured edge couplers.

6 Conclusions and perspectives

This article provides a comprehensive review of subwavelength structured silicon photonic devices. It starts from

the optical properties of subwavelength structured waveguides and then discusses a variety of functional devices implemented with refractive index engineering in 1D and 2D silicon waveguides, including PBSs, PRs, PSRs, polarizers, mode converters, mode multiplexers, waveguide couplers, crossings, bends, grating couplers, and edge couplers. Due to the flexible, wide-range, multidimensional engineering of the refractive index, many novel subwavelength structured devices have been demonstrated or can be envisioned in the future. From the perspective of fabrication techniques, immersion lithography may facilitate the mass fabrication and commercial exploitation of subwavelength structured devices, whereas the improved lithographic resolution of extreme-ultraviolet lithography can extend the operating band from infrared to visible wavelengths. In terms of design principles, transformation optics is a powerful theoretical tool for the design of novel device functions based on subwavelength structured waveguides. With the combination of adiabatic coupling techniques and subwavelength structure–enabled dispersion engineering, ultrabroadband devices are expected to be within reach in the next few years. The anisotropic optical properties of subwavelength structures have rarely been explored so far but will potentially provide another degree of freedom to manipulate the propagation of light at the subwavelength scale [109]. In summary, advanced theoretical analysis and fabrication technologies have significantly facilitated research on subwavelength engineering and paved the way toward future commercialization of these kinds of novel functional devices.

Acknowledgments: This work is supported in part by the State Key Research Development Program of China (Grant No. 2019YFB1803903) and the National Natural Science Foundation of China (Grant Nos. 61835008, 61860206001, 61975115, 61605112, Funder Id: http://dx.doi.org/10.13039/501100001809).

References

[1] Vlasov YA, McNab SJ. Losses in single-mode silicon-on-insulator strip waveguides and bends. Opt Express 2004;12:1622–31.
[2] Cheben P, Schmid J, Delâge A, et al. A high-resolution silicon-on-insulator arrayed waveguide grating microspectrometer with sub-micrometer aperture waveguides. Opt Express 2007;15:2299–306.
[3] Lee J-M, Kim D-J, Kim G-H, et al. Controlling temperature dependence of silicon waveguide using slot structure. Opt Express 2008;16:1645–52.
[4] Lončar M, Doll T, Vučković J, et al. Design and fabrication of silicon photonic crystal optical waveguides. J Lightwave Technol 2000;18:1402–11.
[5] Cheben P, Xu D-X, Janz S, et al. Subwavelength waveguide grating for mode conversion and light coupling in integrated optics. Opt Express 2006;14:4695–702.
[6] Lin S, Hammood M, Yun H, et al. Computational lithography for silicon photonics design. IEEE J Sel Top Quantum Electron 2020;26:8201408.
[7] Novack A, Streshinsky M, Ding R, et al. Progress in silicon platforms for integrated optics. Nanophotonics 2014;3:205–14.
[8] Bojko RJ, Li J, He L, et al. Electron beam lithography writing strategies for low loss, high confinement silicon optical waveguides. J Vac Sci Technol B 2011;29:06F309.
[9] Cheben P, Halir R, Schmid JH, et al. Subwavelength integrated photonics. Nature 2018;560:565–72.
[10] Halir R, Bock PJ, Cheben P, et al. Waveguide sub-wavelength structures: a review of principles and applications. Laser Photon Rev 2015;9:25–49.
[11] Halir R, Ortega-Moñux A, Benedikovic D, et al. Subwavelength-grating metamaterial structures for silicon photonic devices. Proc IEEE 2018;106:2144–57.
[12] Wu H, Li C, Song L, et al. Ultra-sharp multimode waveguide bends with subwavelength gratings. Laser Photon Rev 2019;13:1800119.
[13] Xu H, Shi Y. Metamaterial-based Maxwell's fisheye lens for multimode waveguide crossing. Laser Photon Rev 2018;12:1800094.
[14] Lalanne P, Astilean S, Chavel P, et al. Design and fabrication of blazed binary diffractive elements with sampling periods smaller than the structural cutoff. J Opt Soc Am A 1999;16:1143–56.
[15] Choy TC. Effective medium theory: principles and applications. Vol. 165. New York: Oxford University Press, 2015.
[16] Bock PJ, Cheben P, Schmid JH, et al. Subwavelength grating periodic structures in silicon-on-insulator: a new type of microphotonic waveguide. Opt Express 2010;18:20251–62.
[17] Sakoda K. Optical properties of photonic crystals. Vol. 80. New York, USA: Springer Science & Business Media, 2004.
[18] Lecamp G, Hugonin J-P, Lalanne P. Theoretical and computational concepts for periodic optical waveguides. Opt Express 2007;15:11042–60.
[19] Ctyroky J. 3-D bidirectional propagation algorithm based on Fourier series. J Lightwave Technol 2012;30:3699–708.
[20] Rytov S. Electromagnetic properties of a finely stratified medium. Soviet Physics JEPT 1956;2:466–75.
[21] Wang Z, Xu X, Fan D, et al. Geometrical tuning art for entirely subwavelength grating waveguide based integrated photonics circuits. Sci Rep 2016;6:24106.
[22] Xu H, Shi Y. Ultra-sharp multi-mode waveguide bending assisted with metamaterial-based mode converters. Laser Photon Rev 2018;12:1700240.
[23] Vasić B, Isić G, Gajić R, et al. Controlling electromagnetic fields with graded photonic crystals in metamaterial regime. Opt Express 2010;18:20321–33.
[24] Hunt J, Tyler T, Dhar S, et al. Planar, flattened Luneburg lens at infrared wavelengths. Opt Express 2012;20:1706–13.
[25] Barwicz T, Watts MR, Popović MA, et al. Polarization-transparent microphotonic devices in the strong confinement limit. Nat Photonics 2007;1:57–60.

[26] Qiu H, Su Y, Yu P, et al. Compact polarization splitter based on silicon grating-assisted couplers. Opt Lett 2015;40:1885–7.
[27] Zhang Y, He Y, Wu J, et al. High-extinction-ratio silicon polarization beam splitter with tolerance to waveguide width and coupling length variations. Opt Express 2016;24:6586–93.
[28] Liu L, Deng Q, Zhou Z. Manipulation of beat length and wavelength dependence of a polarization beam splitter using a subwavelength grating. Opt Lett 2016;41:5126–9.
[29] Xu Y, Xiao J. Compact and high extinction ratio polarization beam splitter using subwavelength grating couplers. Opt Lett 2016;41:773–6.
[30] Zhang J, Yang J, Liang L, et al. Broadband TM-mode-pass polarizer and polarization beam splitter using asymmetrical directional couplers based on silicon subwavelength grating. Opt Commun 2018;407:46–50.
[31] Guo Z, Xiao J. Ultracompact silicon-based polarization beam splitter using subwavelength gratings. IEEE Photonics Technol Lett 2017;29:1800–3.
[32] Xu H, Dai D, Shi Y. Ultra-broadband and ultra-compact on-chip silicon polarization beam splitter by using hetero-anisotropic metamaterials. Laser Photon Rev 2019;13:1800349.
[33] Wu S, Xiao J. Compact polarization rotator for silicon-based cross-slot waveguides using subwavelength gratings. Appl Optics 2017;56:4892–9.
[34] Xu H, Shi Y. Subwavelength-grating-assisted silicon polarization rotator covering all optical communication bands. Opt Express 2019;27:5588–97.
[35] Xiong Y, Wanguemert-Perez JG, Xu D, et al. Polarization splitter and rotator with subwavelength grating for enhanced fabrication tolerance. Opt Lett 2014;39:6931–4.
[36] He Y, Zhang Y, Wang X, et al. Silicon polarization splitter and rotator using a subwavelength grating based directional coupler. In: Optical Fiber Communication Conference (OFC), Th1G.6. San Francisco, CA, USA: Optical Society of America; 2017.
[37] Wang Y, Ma M, Yun H, et al. Ultra-compact sub-wavelength grating polarization splitter-rotator for silicon-on-insulator platform. IEEE Photonics J 2016;8:7805709.
[38] Xu Y, Xiao J. Ultracompact and high efficient silicon-based polarization splitter-rotator using a partially-etched subwavelength grating coupler. Sci Rep 2016;6:27949.
[39] Guan X, Chen P, Chen S, et al. Low-loss ultracompact transverse-magnetic-pass polarizer with a silicon subwavelength grating waveguide. Opt Lett 2014;39:4514–7.
[40] Xu H, Dai D, Shi Y. Anisotropic metamaterial-assisted all-silicon polarizer with 415-nm bandwidth. Photonics Res 2019;7:1432–9.
[41] Shahin M, Gevorgyan H, Dahlem MS, et al. TM-polarizer using segmented silicon waveguide. In: Integrated Photonics Research, Silicon and Nanophotonics (IPRSN), IM2A.4. Boston, USA: Optical Society of America; 2015.
[42] Xiong Y, Xu D, Schmid JH, et al. High extinction ratio and broadband silicon TE-pass polarizer using subwavelength grating index engineering. IEEE Photonics J 2015;7:7802107.
[43] He Y, Zhang Y, Jiang X, et al. On-chip silicon three-mode (de) multiplexer employing subwavelength grating structure. In: European Conference on Optical Communication (ECOC). Gothenburg, Sweden: IEEE; 2017.
[44] He Y, Zhang Y, Zhu Q, et al. Silicon high-order mode (de) multiplexer on single polarization. J Lightwave Technol 2018;36:5746–53.
[45] Dave UD, Lipson M. Efficient conversion to very high order modes in silicon waveguides. In: Conference on Lasers and Electro-Optics (CLEO), SM3J. 6. San Jose, CA, USA: Optical Society of America; 2019.
[46] Xu L, Wang Y, Mao D, et al. Ultra-broadband and compact two-mode multiplexer based on subwavelength-grating-slot–assisted adiabatic coupler for the silicon-on-insulator platform. J Lightwave Technol 2019;37:5790–800.
[47] Pérez-Galacho D, Marris-Morini D, Ortega-Moñux A, et al. Add/drop mode-division multiplexer based on a Mach–Zehnder interferometer and periodic waveguides. IEEE Photonics J 2015;7:7800907.
[48] Pérez-Galacho D, Marris-Morini D, Ortega-Moñux A, et al. Mode filtering in periodic waveguides by means of band gap engineering. In: Optical Interconnects Conference (OI), 68–9. San Jose, CA, USA: IEEE; 2015.
[49] Pérez-Galacho D, Marris-Morini D, Ortega-Moñux A, et al. Broadband add/drop mode division multiplexer based on a Mach–Zehnder interferometer. In: The 12th International Conference on Group IV Photonics (GFP), 98–9. Vancouver, British Columbia, Canada: IEEE; 2015.
[50] González-Andrade D, Wangüemert-Pérez JG, Velasco AV, et al. Ultra-broadband mode converter and multiplexer based on sub-wavelength structures. IEEE Photonics J 2018;10:2201010.
[51] González-Andrade D, Velasco AV, Wangüemert-Pérez J, et al. Ultra-broadband mode (de)multiplexer based on a sub-wavelength engineered MMI coupler. In: IEEE Photonics Conference (IPC), 423–4. Orlando, FL, USA: IEEE; 2017.
[52] González-Andrade D, Wangüemert-Pérez J, Velasco AV, et al. Ultra-broadband mode converter and multiplexer using a sub-wavelength metamaterial. In: European Conference on Optical Communication (ECOC). Rome, Italy: IEEE; 2018.
[53] Okamoto K. Fundamentals of optical waveguides. San Diego: Academic Press, 2006.
[54] Ohana D, Levy U. Mode conversion based on dielectric metamaterial in silicon. Opt Express 2014;22:27617–31.
[55] Ohana D, Desiatov B, Mazurski N, et al. Dielectric metasurface as a platform for spatial mode conversion in nanoscale waveguides. Nano Lett 2016;16:7956–61.
[56] Li Z, Kim M-H, Wang C, et al. Controlling propagation and coupling of waveguide modes using phase-gradient metasurfaces. Nat Nanotechnol 2017;12:675–83.
[57] Wang H, Zhang Y, He Y, et al. Compact silicon waveguide mode converter employing dielectric metasurface structure. Adv Opt Mater 2019;7:1801191.
[58] Cheng Z, Wang J, Yang Z, et al. Sub-wavelength grating assisted mode order converter on the SOI substrate. Opt Express 2019;27:34434–41.
[59] Xiao R, Shi Y, Li J, et al. On-chip mode converter based on two cascaded Bragg gratings. Opt Express 2019;27:1941–57.
[60] He Y, Zhang Y, Wang H, et al. On-chip silicon mode blocking filter employing subwavelength-grating based contra-directional coupler. Opt Express 2018;26:33005–12.
[61] Jiang W, Miao J, Li T, et al. Low-loss and broadband silicon mode filter using cascaded plasmonic BSWGs for on-chip mode division multiplexing. Opt Express 2019;27:30429–40.
[62] Dai D, Bowers JE. Silicon-based on-chip multiplexing technologies and devices for Peta-bit optical interconnects. Nanophotonics 2014;3:283–311.

[63] Halir R, Maese-Novo A, Ortega-Moñux A, et al. Compact broadband directional coupler. In: The 9th International Conference on Group IV Photonics (GFP), 177–9. San Diego, CA, USA: IEEE; 2012.
[64] Ortega-Monux A, Zavargo-Peche L, Maese-Novo A, et al. High-performance multimode interference coupler in silicon waveguides with subwavelength structures. IEEE Photonics Technol Lett 2011;23:1406–8.
[65] Lu L, Liu D, Yan M, et al. Subwavelength adiabatic multimode Y-junctions. Opt Lett 2019;44:4729–32.
[66] Benedikovic D, Berciano M, Alonso-Ramos C, et al. Dispersion control of silicon nanophotonic waveguides using sub-wavelength grating metamaterials in near- and mid-IR wavelengths. Opt Express 2017;25:19468–78.
[67] Halir R, Maese-Novo A, Ortega-Moñux A, et al. Colorless directional coupler with dispersion engineered sub-wavelength structure. Opt Express 2012;20:13470–7.
[68] Yun H, Wang Y, Zhang F, et al. Broadband 2×2 adiabatic 3 dB coupler using silicon-on-insulator sub-wavelength grating waveguides. Opt Lett 2016;41:3041–4.
[69] Halir R, Cheben P, Luque-González JM, et al. Ultra-broadband nanophotonic beam splitter using an anisotropic sub-wavelength metamaterial. Laser Photon Rev 2016;10:1039–46.
[70] Wang Y, Lu Z, Ma M, et al. Compact broadband directional couplers using subwavelength gratings. IEEE Photonics J 2016;8:7101408.
[71] Xu L, Wang Y, Kumar A, et al. Compact high-performance adiabatic 3-dB coupler enabled by subwavelength grating slot in the silicon-on-insulator platform. Opt Express 2018;26:29873–85.
[72] Xu H, Shi Y. Ultra-compact polarization-independent directional couplers utilizing a subwavelength structure. Opt Lett 2017;42:5202–5.
[73] Soldano LB, Pennings ECM. Optical multi-mode interference devices based on self-imaging: principles and applications. J Lightwave Technol 1995;13:615–27.
[74] Maese-Novo A, Halir R, Romero-García S, et al. Wavelength independent multimode interference coupler. Opt Express 2013;21:7033–40.
[75] Dong P, Xiang L, Chandrasekhar S, et al. Monolithic silicon photonic integrated circuits for compact 100+ Gb/s coherent optical receivers and transmitters. IEEE J Sel Top Quantum Electron 2014;20:150–7.
[76] Xu L, Wang Y, Patel D, et al. Ultra-broadband and ultra-compact optical 90° hybrid based on 2×4 MMI coupler with subwavelength gratings on silicon-on-insulator. In: Optical Fiber Communication Conference (OFC), M3I.7. San Diego, CA, USA: Optical Society of America; 2018.
[77] Bock PJ, Cheben P, Schmid JH, et al. Subwavelength grating crossings for silicon wire waveguides. Opt Express 2010;18:16146–55.
[78] Wu Q, Turpin JP, Werner DH. Integrated photonic systems based on transformation optics enabled gradient index devices. Light-Sci Appl 2012;1:e38.
[79] Zhang Y, Hosseini A, Xu X, et al. Ultralow-loss silicon waveguide crossing using Bloch modes in index-engineered cascaded multimode-interference couplers. Opt Lett 2013;38:3608–11.
[80] Xu L, Chen H. Conformal transformation optics. Nat Photonics 2015;9:15–23.
[81] Valentine J, Li J, Zentgraf T, et al. An optical cloak made of dielectrics. Nat Mater 2009;8:568–71.
[82] Luque-González JM, Halir R, Wangüemert-Pérez JG, et al. An ultracompact GRIN-lens-based spot size converter using subwavelength grating metamaterials. Laser Photon Rev 2019;13:1900172.
[83] Li S, Zhou Y, Dong J, et al. Universal multimode waveguide crossing based on transformation optics. Optica 2018;5:1549–56.
[84] Zentgraf T, Valentine J, Tapia N, et al. An optical "Janus" device for integrated photonics. Adv Mater 2010;22:2561–4.
[85] Merchand E. Gradient Index Optics. New York: Academic Press; 1978.
[86] Garnett J, Valentine J. Maxwell fisheye lens as a waveguide crossing for integrated photonics. In: Conference on Lasers and Electro-Optics (CLEO), JW4A.88. San Diego, CA, USA: Optical Society of America; 2012.
[87] Badri SH, Gilarlue MM, Soofi H, et al. 3×3 slot waveguide crossing based on Maxwell's fisheye lens. Opt Eng 2019;58:097102.
[88] Xu Q, Fattal D, Beausoleil RG. Silicon microring resonators with 1.5-μm radius. Opt Express 2008;16:4309–15.
[89] Gabrielli LH, Liu D, Johnson SG, et al. On-chip transformation optics for multimode waveguide bends. Nat Commun 2012;3:1217.
[90] Benedikovic D, Cheben P, Schmid JH, et al. High-efficiency single etch step apodized surface grating coupler using subwavelength structure. Laser Photon Rev 2014;8:L93–7.
[91] Cheben P, Schmid JH, Wang S, et al. Broadband polarization independent nanophotonic coupler for silicon waveguides with ultra-high efficiency. Opt Express 2015;23:22553–63.
[92] Alonso-Ramos C, Cheben P, Ortega-Moñux A, et al. Fiber-chip grating coupler based on interleaved trenches with directionality exceeding 95%. Opt Lett 2014;39:5351–4.
[93] Watanabe T, Fedoryshyn Y, Leuthold J. 2-D grating couplers for vertical fiber coupling in two polarizations. IEEE Photonics J 2019;11:1–9.
[94] Benedikovic D, Alonso-Ramos C, Cheben P, et al. Single-etch subwavelength engineered fiber-chip grating couplers for 1.3 μm Datacom wavelength band. Opt Express 2016;24:12893–904.
[95] Benedikovic D, Alonso-Ramos C, Pérez-Galacho D, et al. L-shaped fiber-chip grating couplers with high directionality and low reflectivity fabricated with deep-UV lithography. Opt Lett 2017;42:3439–42.
[96] Zhang Z, Chen X, Cheng Q, et al. High-efficiency apodized bidirectional grating coupler for perfectly vertical coupling. Opt Lett 2019;44:5081–4.
[97] Benedikovic D, Cheben P, Schmid JH, et al. Subwavelength index engineered surface grating coupler with sub-decibel efficiency for 220-nm silicon-on-insulator waveguides. Opt Express 2015;23:22628–35.
[98] Xu X, Subbaraman H, Covey J, et al. Colorless grating couplers realized by interleaving dispersion engineered subwavelength structures. Opt Lett 2013;38:3588–91.
[99] Zhong Q, Veerasubramanian V, Wang Y, et al. Focusing-curved subwavelength grating couplers for ultra-broadband silicon photonics optical interfaces. Opt Express 2014;22:18224–31.
[100] Wang Y, Shi W, Wang X, et al. Design of broadband subwavelength grating couplers with low back reflection. Opt Lett 2015;40:4647–50.
[101] Ong EW, Wallner T, Fahrenkopf NM, et al. High positional freedom SOI subwavelength grating coupler (SWG) for 300 mm foundry fabrication. Opt Express 2018;26:28773–92.

[102] Cheben P, Bock PJ, Schmid JH, et al. Refractive index engineering with subwavelength gratings for efficient microphotonic couplers and planar waveguide multiplexers. Opt Lett 2010;35:2526–8.
[103] Barwicz T, Boyer N, Janta-Polczynski A, et al. A metamaterial converter centered at 1490nm for interfacing standard fibers to nanophotonic waveguides. In: Optical Fiber Communication Conference (OFC). Los Angeles, CA, USA: IEEE; 2016:1–3.
[104] Barwicz T, Peng B, Leidy R, et al. Integrated metamaterial interfaces for self-aligned fiber-to-chip coupling in volume manufacturing. IEEE J Sel Top Quantum Electron 2018;25:1–13.
[105] Papes M, Cheben P, Benedikovic D, et al. Fiber-chip edge coupler with large mode size for silicon photonic wire waveguides. Opt Express 2016;24:5026–38.
[106] Wang X, Quan X, Liu M, et al. Silicon-nitride-assisted edge coupler interfacing with high numerical aperture fiber. IEEE Photonics Technol Lett 2019;31:349–52.
[107] Moura U, Bustamante Y, Farias G, et al. Design and optimization of subwavelength silicon photonics edge coupler for cleaved fibers. In: SBFoton International Optics and Photonics Conference (SBFoton IOPC). Campinas, Brazil: IEEE; 2018:1–5.
[108] Barwicz T, Kamlapurkar S, Martin Y, et al. A silicon metamaterial chip-to-chip coupler for photonic flip-chip applications. In: Optical Fiber Communication Conference (OFC), Th2A. 39. Optical Society of America; 2017.
[109] Luque-González JM, Herrero-Bermello A, Ortega-Moñux A, et al. Tilted subwavelength gratings: controlling anisotropy in metamaterial nanophotonic waveguides. Opt Lett 2018;43:4691–4.